Chinese Journal of
POLYMER SCIENCE

RESEARCH ARTICLE

https://doi.org/10.1007/s10118-026-3611-z
Chinese J. Polym. Sci.

Polyoxometalate-doped Chitosan Quaternary Ammonium/ Polyacrylamide Interpenetrating Hydrogels with Enhanced Mechanical and Tribological Properties

Fang Xu[a], Xin-Bao Han[b], Hao-Hao Ren[a], Wei-Tao Gong[a,c], Rong-Sheng Cai[a], Yu Li[a], Ming Zhang[a*], and Wen-Bo Sheng[a,d*]

[a] *State Key Laboratory of Solid Lubrication, Lanzhou Institute of Chemical Physics, Chinese Academy of Sciences, Lanzhou 730000, China*
[b] *College of Chemistry and Chemical Engineering, Lanzhou University, Lanzhou 730000, China*
[c] *School of Stomatology, Lanzhou University, Lanzhou 730000, China*
[d] *Shandong Laboratory of Advanced Materials and Green Manufacturing at Yantai, Yantai 264000, China*

Electronic Supplementary Information

Abstract Combining nanomaterials with the three-dimensional hydrophilic network of hydrogels is an effective strategy for creating smart materials with enhanced mechanical properties and advanced functionalities. Herein, chitosan quaternary ammonium/polyacrylamide (QP) hydrogels with interpenetrating networks were prepared *via* an *in situ* method based on chain entanglement, in which polyoxometalate (POM) nanoparticles were introduced as physical crosslinking agents. This incorporation of POMs significantly improved the overall mechanical properties of the hydrogels, endowing them with high fracture energy, low hysteresis, and outstanding resilience under high water content (>90%). Owing to the strong water molecule adsorption capacity of POMs and their homogeneous and dense distribution as physical crosslinking points in the hydrogel structure, the friction coefficient was significantly reduced. Furthermore, the hydrogels exhibited good biocompatibility as well as pH- and ion-responsive behavior, while maintaining structural stability under varying external stimuli. Notably, the swelling ratio increased in high-concentration salt solutions, making them promising for applications in controlled drug release, intelligent monitoring, and especially in seawater desalination treatment.

Keywords Polyoxometalates; Hydrogel; Chain entanglement; Low friction; Stimuli responsiveness

Citation: Xu, F.; Han, X. B.; Ren, H. H.; Gong, W. T.; Cai, R. S.; Li, Y.; Zhang, M.; Sheng, W. B. Polyoxometalate-doped chitosan quaternary ammonium/polyacrylamide interpenetrating hydrogels with enhanced mechanical and tribological properties. *Chinese J. Polym. Sci.* https://doi.org/10.1007/s10118-026-3611-z

INTRODUCTION

Since their initial report in the 1960s, hydrogels have demonstrated significant application potential in fields such as biomedicine, flexible electronics, and environmental engineering because their soft and moist properties are similar to those of biological tissues.[1,2] In recent years, with the rapid advancement of materials science and engineering technologies, hydrogel research has progressed toward multifunctionality and intelligence. Through molecular design, composite modification, and microstructural regulation, a variety of advanced hydrogels with high strength, toughness, self-healing capabilities, and environmental responsiveness have been successfully developed. Meanwhile, the application boundaries of hydrogels continue to expand, driving progress in regenerative medicine and precision therapy,[3,4] and providing versatile platforms for wearable devices, human-machine interfaces, and biomimetic sensors,[5,6] with growing relevance to daily life, water resource management, and environmental protection.[7,8] Among various hydrogel systems, composite hydrogels are one of the most active research directions. By integrating multiple components with distinct structures and functions, composite hydrogels can achieve hierarchical architectures and synergistic effects, thereby exhibiting properties that are difficult to realize in conventional single-component hydrogels, while preserving their intrinsic softness and high water content.

Currently, research on composite hydrogels is primarily focused on mechanical enhancement, functional integration, and bioinspired structural design, among which material doping plays a crucial role.[9] The introduction of nanomaterials such as graphene, carbon nanotubes, and cellulose nanocrystals can significantly improve the strength, toughness, fatigue resistance, and self-healing capabilities of hydrogels.[10–13] In addition, integrating conductive materials (*e.g.*, PEDOT:PSS, MXene) enables applications in flexible sensors

* Corresponding authors, E-mail: zhm@licp.cas.cn (M.Z.)
E-mail: shengwb@licp.cas.cn (W.B.S.)
Received January 3, 2026; Accepted February 4, 2026; Published online April 16, 2026

and bioelectrodes.[14,15] The incorporation of magnetic nanoparticles (*e.g.*, Fe_3O_4) facilitates magnetothermal therapy and magnetically controlled motion.[16] Furthermore, photothermal materials, including polydopamine and gold nanorods, have been employed to confer photoresponsive behavior and photothermal therapeutic functions.[17]

Polyoxometalates (POMs), a class of metal-oxygen cluster compounds with atomically precise structures, typically exist as polyanions and exhibit good solubility in water and other polar solvents. Owing to these characteristics, POMs can act as dynamic or physical crosslinking enhancers through electrostatic interactions with cationic polymer chains or ion-bridging effects.[18–20] For example, Li *et al*.[21] reported that an appropriate amount of $H_3PW_{12}O_{40}$ could effectively enhance the network density owing to the crosslinking effect, thereby improving the tensile strength. However, excessive POMs loading may lead to an uneven distribution of the network structure and pronounced electrostatic repulsion, hindering effective crosslinking with polymer chains and consequently reducing the fracture stress. Beyond their structural role, POMs are also responsive to various external stimuli, including light, electric fields, and redox conditions,[22–24] and exhibit biological activities such as antibacterial, anti-inflammatory, and antiviral effects,[25–27] making them attractive for applications in smart sensing and biomaterials.

In our previous research,[28] POMs were doped into carboxymethyl chitosan-based hydrogel systems, where they could form physical cross-links through hydrogen bonding. However, as polyanionic clusters, POMs also serve as excellent mediators of the electrostatic interactions. Additionally, in prior studies, we observed abnormal swelling behavior of the hydrogels in salt solutions, which is interesting and valuable for further investigation. In this study, chitosan quaternary ammonium/polyacrylamide (QP) hydrogels with interpenetrating network structures were prepared *via in situ* polymerization. The resulting hydrogel network contained abundant chain entanglement, which provided an intrinsic basis for mechanical robustness. By doping POMs as a physical crosslinking agent, the mechanical properties of the hydrogels were effectively enhanced, endowing them with high fracture energy and excellent resilience under high water content conditions. Moreover, the POM-doped hydrogel QPP retained favorable biocompatibility. Because of the strong water adsorption capacity of the POMs, the friction coefficient of the hydrogels was significantly reduced. In addition, the QPP hydrogels exhibited pronounced pH- and ion-responsive behavior. Notably, its ability to increase the swelling ratio in high-concentration salt solutions, which usually only appears in zwitterionic hydrogels, makes it a promising candidate for seawater desalination applications.

EXPERIMENTAL

Materials

Chitosan quaternary ammonium (QCS degree of substitution: 98%, Macklin), acrylamide (AM, ≧99%, J&K Scientific), *N,N'*-methylene-bisacrylamide (MBAA, 99%, Sigma-Aldrich), lithium phenyl-2,4,6-trimethylbenzoylphosphinate (LAP, 95%, Sigma-Aldrich), and hydrochloric acid (HCl, 36%–38%, Rionlon Bohua, China) were utilized without further purification. Sodium chloride (NaCl), potassium chloride (KCl), ammonium chloride (NH_4Cl), calcium chloride ($CaCl_2$), magnesium sulfate ($MgSO_4$), aluminum chloride hexahydrate ($AlCl_3{\cdot}6H_2O$), and sodium hydroxide (NaOH) purchased from Chengdu Kelong Chemical Reagent Co., Ltd. POMs ($Mo_{72}V_{30}$) were synthesized according to the literature[29,30] by Xinbao Han.

Molecular structure: $Na_8K_{14}(VO)_2[\{(Mo^{VI})Mo^{VI}_5O_{21}(H_2O)_3\}_{10}\{(Mo^{VI})Mo^{VI}_5O_{21}(H_2O)_3(SO_4)\}_2\{V^{IV}O(H_2O)\}_{20}\{V^{IV}O\}_{10}(\{KSO_4\}_5)_2{\cdot}{\approx}150\ H_2O$. Fourier transform infrared (FTIR) (KBr pellet, 400–4000 cm^{-1}): 1613 (m, δ_{H_2O}), 1200, 1127, 1056 ($\nu_{as(SO_4)}$), 965, 791, 630, 575, 446 cm^{-1}.

Preparation of QP and QPP Hydrogels

A series of $Mo_{72}V_{30}$ aqueous solutions (10 mL) with different concentrations (0, 0.014, 0.034, 0.069, 0.137 $mg{\cdot}mL^{-1}$) were prepared in advance. AM (7.10 g), QCS (0.71 g), photoinitiator (LAP, 0.02 wt% of AM), and crosslinker (MBAA, 0.1 wt% of AM) were subsequently added to the $Mo_{72}V_{30}$ solutions. The resulting mixture was stirred in the dark until homogeneous and transparent precursor solutions were obtained. After degassing by ultrasonication to remove bubbles, the precursor solution was poured into molds composed of double-layer glass plates separated by a polytetrafluoroethylene (PTFE) spacer. Photopolymerization was performed under UV light (365 nm) for 40 min at room temperature. The formed hydrogels were immersed in deionized water until the swelling equilibrium was reached. The hydrogel prepared without $Mo_{72}V_{30}$ was recorded as QP, whereas the $Mo_{72}V_{30}$-doped hydrogels were recorded as QPP_{20} (0.014 $mg{\cdot}mL^{-1}$), QPP_{50} (0.034 $mg{\cdot}mL^{-1}$), QPP_{100} (0.069 $mg{\cdot}mL^{-1}$), and QPP_{200} (0.137 $mg{\cdot}mL^{-1}$).

Characterizations

Fourier transform infrared (FTIR) spectra were obtained using a Fourier spectrometer (Nicolet iS10, Thermo Fisher Scientific Inc., USA). High-resolution transmission electron microscopy (HRTEM) images were acquired using a Thermo Fisher Scientific Spectra 300 microscope equipped with a Schottky-type field-emission gun and a GATAN OneView CCD camera (model 1095). The morphology of the hydrogels was observed by scanning electron microscopy (SEM) FEI Quanta 650 FEG (USA). Elemental mapping was performed using a JSM-5601LV scanning electron microscopy.

Tensile and Compressive Test

Tensile and compressive tests were conducted using an EZ-Test (Shimadzu, Japan) universal testing machine with a 500 N load cell at crosshead loading speeds of 20 and 5 $mm{\cdot}min^{-1}$, respectively. All hydrogels were subjected to mechanical property testing after reaching swelling equilibrium. The fracture energy ($kJ{\cdot}m^{-3}$) of the hydrogel was calculated by integrating the area under the tensile stress-strain curve using Eq. (1):

$$W = \int_{\varepsilon=0}^{\varepsilon=\varepsilon_b} \sigma_b d\varepsilon \quad (1)$$

where σ_b and ε_b are the tensile strength and corresponding fracture elongation, respectively. Young's modulus (kPa) was determined from the slope of the linear between 5% and 15% strain of the stress-strain curve. The fatigue resistance of the hydrogel was investigated by measuring the continuous loading-unloading tensile hysteresis under a fixed strain, with the loading speed set at 100 $mm{\cdot}min^{-1}$.

https://doi.org/10.1007/s10118-026-3611-z

Swelling Test

The swelling ratio (SR) was calculated as follows:

$$SR = \frac{m_i - m_0}{m_0} \times 100\% \quad (2)$$

where m_i and m_0 are the weight of equilibrium-swollen and dried hydrogels. In the swelling kinetics experiments, the hydrogels were periodically removed from the deionized water at consecutive time intervals. The surface moisture was blotted with a filter paper, and the weight was recorded until no further change was observed. Three parallel samples were measured, and the final data are presented as mean ± SD. To observe the moisture absorption capacity of the hydrogels, they were placed in a sealed chamber, where the relative humidity was controlled at 85% at 25 °C using a saturated KCl solution, and the weight change of the hydrogels was recorded.

pH- and Ion-responsiveness

Dried hydrogel samples were immersed in buffer solutions with pH values ranging from 2 to 12 at room temperature for seven days. After immersion, the samples were removed and excess surface water was gently blotted with filter paper prior to weighing. The SR was calculated to evaluate the pH responsiveness of the hydrogels. For the pH-responsive cycle-swelling tests, the soaking time interval was 30 min. To investigate ion-responsive swelling behavior, the hydrogels were immersed in aqueous salt solutions (NaCl, KCl, NH_4Cl, $CaCl_2$, $MgSO_4$, and $AlCl_3{\cdot}6H_2O$) at concentration of 0.9 wt% and 20 wt% at room temperature. After 48 h of immersion, the samples were removed, the surface moisture was wiped off with filter paper, and the samples were weighed to determine the SR. For ion-responsive cycle swelling experiments, the soaking time for each cycle was set to 5 h.

Friction Test

Friction tests were performed using a conventional ball-on-disk reciprocating tribometer (CSM Co., Ltd., Switzerland) by recording the friction coefficient. For the ball-on-disk test, a polydimethylsiloxane (PDMS) ball was used as the contact pair, hydrogels were used as test substrates, and deionized water was used as the lubricant. The applied load and sliding frequency were set to 0.5 N and 1 Hz, respectively, and the distance of one sliding cycle was 5 mm.

Biocompatibility Evaluation

CCK-8 Assay: the hydrogel was placed in DMEM medium containing 10% fetal bovine serum (FBS) at 4 °C for 24 h to collect the hydrogel leach liquor for further use. The ratio of the hydrogel to DMEM was 0.1 g·mL^{-1}. Mouse L929 fibroblast cells were pipetted into a 96-well plate (4000 cells per well, n=4) and incubated for 12 h until the cells adhered to the plate. The culture medium was then discarded. Cells were treated with hydrogel leach liquor (100 μL per well) and incubated for 24, 48, or 72 h at 37 °C with 5% CO_2. At each time point, 90 μL of DMEM was supplemented with 10 μL of CCK-8 reagent and added to each well. After 1 h of incubation, absorbance was measured at 450 nm using an enzyme marker (Tecan, Switzerland).

Live/dead Cell Staining Assay: Mouse L929 fibroblast cells were pipetted into a 96-well plate (4000 cells per well, n=4) and incubated for 12 h until the cells adhered to the plate. The culture medium was then discarded. Cells were treated with hydrogel leach liquor (100 μL per well) and incubated for 24, 48, or 72 h at 37 °C with 5% CO_2. The samples were then stained with a Calcein-AM/PI kit for the visualization of live and dead cells under an inverted fluorescence microscope.

RESULTS AND DISCUSSION

Synthesis and Characterization of Hydrogels.

The chemical structures of QCS, AM, MBAA, and $Mo_{72}V_{30}$, and a schematic of the fabrication process are shown in Scheme 1. In

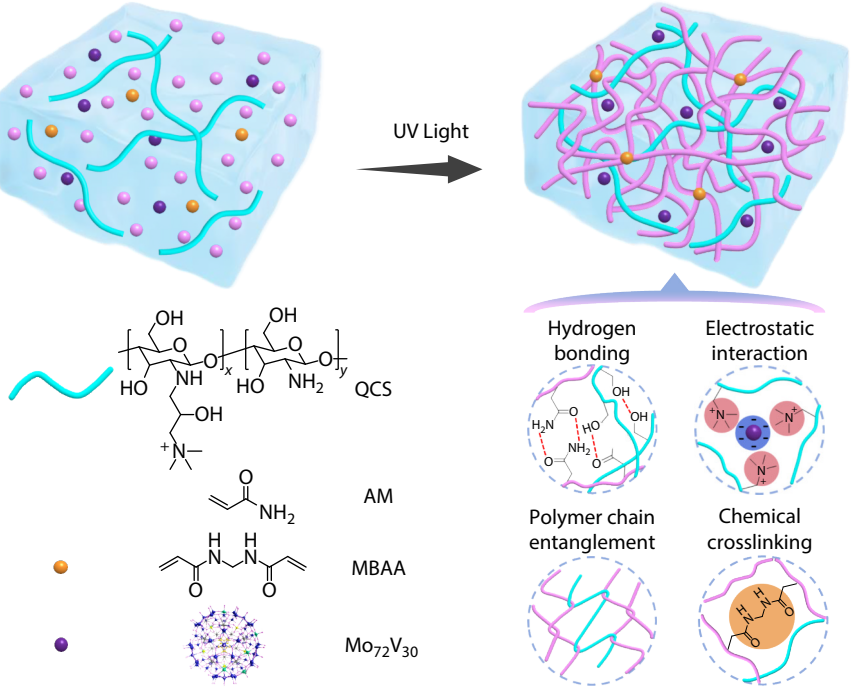

Scheme 1 The synthesis mechanism for QPP hydrogels.

https://doi.org/10.1007/s10118-026-3611-z

the QPP hydrogels, a low content of crosslinker and initiator, combined with a high monomer concentration, was employed, favoring the formation of an entangled polymer network.[31] As a result, abundant hydrogen-bonding interactions were established among the densely packed polymer chains. In addition, the incorporation of $Mo_{72}V_{30}$ introduced additional electrostatic interactions between the negatively charged POMs and the quaternary ammonium cation of QCS. The HRTEM image (Fig. 1a) reveals that $Mo_{72}V_{30}$ exists in the form of nanoscale particles. The as-prepared hydrogels exhibited excellent optical transparencies (Fig. S1 in the electronic supplementary information, ESI), indicating a homogeneous distribution of components within the hydrogels. The FTIR spectra of QCS, MA, $Mo_{72}V_{30}$, dried QP, and QPP hydrogels are shown in Fig. 1(b). Compared with the AM monomer, the N—H bending vibration band of PAM in both the QP and QPP hydrogels shifts from 1615 cm^{-1} to 1600 cm^{-1}. Meanwhile, the N—H stretching vibration band around 3360 cm^{-1} shifted to lower wavenumbers and broadened, indicating the presence of strong intermolecular hydrogen bonding interactions.[32] $Mo_{72}V_{30}$ exhibits characteristic absorption bands at 965 and 791 cm^{-1}, which are attributed to M=O and M—O—M (M = Mo, V). The characteristic band of the quaternary ammonium salt in QCS is 1480 cm^{-1} but disappears in the QPP hydrogel. Meanwhile, the M=O (M = Mo, V) peak in $Mo_{72}V_{30}$ shifts to 938 cm^{-1}. This is attributed to the strong electrostatic interaction between the negatively charged $Mo_{72}V_{30}$ unit and positively charged QCS.[33–35] The morphology of the hydrogels can be observed by SEM after lyophilization. As shown in Fig. 1(c), the QP hydrogel exhibits interconnected and loosely porous microstructures. In contrast, the QPP hydrogels showed relatively regular and well-defined transverse and longitudinal microstructures, which can be attributed to the formation of electrostatic interactions. Furthermore, with increasing amounts of $Mo_{72}V_{30}$, the porous structure became progressively denser, reflecting the enhanced physical crosslinking effect. EDS mapping results (Fig. 1d) demonstrated that the hydrogels were mainly composed of C, O, and N, while trace amounts of Mo were also detected. Moreover, the EDS mapping images showed that $Mo_{72}V_{30}$ was homogeneously distributed in the hydrogels.

Mechanical Properties

The water content and mechanical properties of hydrogels exhibit a fundamental trade-off relationship, in which an increase in water content often leads to deterioration in mechanical strength. To overcome this paradox, we adopted a combined strategy of optimizing crosslinking and constructing heterogeneous networks by introducing chain entanglement structures

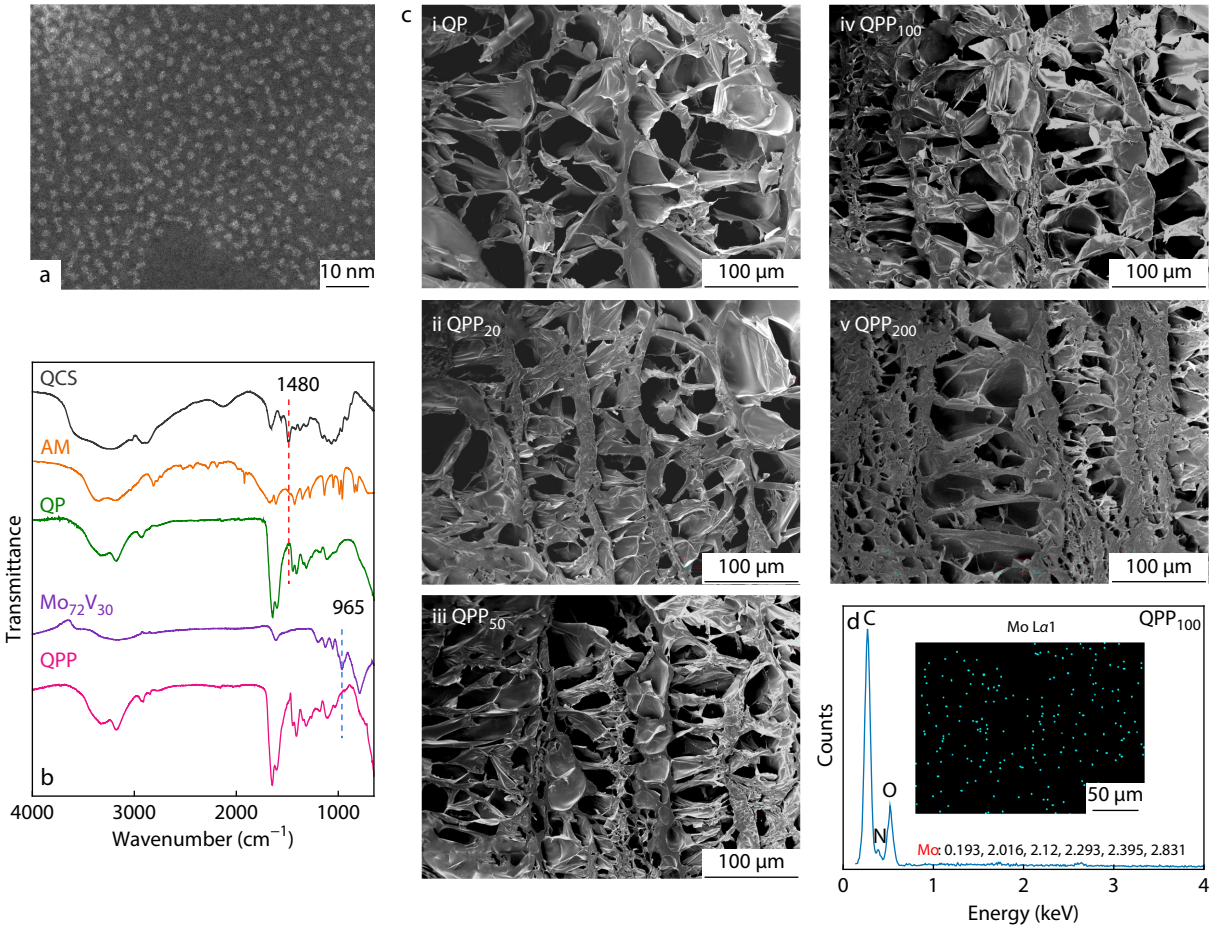

Fig. 1 (a) HRTEM image of $Mo_{72}V_{30}$; (b) FTIR spectra of raw materials and synthetic hydrogels of QP and QPP; (c) SEM images of QPP hydrogels with different concentration of $Mo_{72}V_{30}$: (i) QP (0 mg·mL^{-1}), (ii) QPP_{20} (0.014 mg·mL^{-1}), (iii) QPP_{50} (0.034 mg·mL^{-1}), (iv) QPP_{100} (0.069 mg·mL^{-1}), and (v) QPP_{200} (0.137 mg·mL^{-1}); (d) EDS energy spectrum and mapping image of QPP_{100}.

https://doi.org/10.1007/s10118-026-3611-z

and doping with POMs. From Fig. S2 (in ESI), it can be seen that doping of a small amount of $Mo_{72}V_{30}$ (0.014 mg·mL^{-1}) increases the swelling ratio due to its strong adsorption ability for water molecules. However, a higher $Mo_{72}V_{30}$ content increased the number of physical cross-linking points, enhancing the crosslinking density and consequently reducing the equilibrium swelling ratio. Nevertheless, the water content of all samples remained above 90%. Mechanical tests were subsequently performed on the fully swollen hydrogels with different $Mo_{72}V_{30}$ concentrations and the blank QP sample at room temperature.

The tensile stress-strain curves (Fig. 2a) show that the maximum stress increased from 92 kPa (QP) to 180 kPa (QPP_{100}), and the stretch ratio at rupture increased from 282% to 422%. An appropriate amount of $Mo_{72}V_{30}$ ensured a uniform dispersion within the hydrogel polymer network. During stretching, it acts as an effective cross-linking point to transfer stress, thereby simultaneously enhancing both tensile strength and elongation at break. However, when the $Mo_{72}V_{30}$ addition was further increased to 0.137 mg·mL^{-1}, the tensile performance declined because of the disruption of homogeneous cross-linking in the polymer network itself. This is supported by the SEM images (Fig. 1c), which show that the network structure of QPP_{200} became heterogeneous, exhibiting distinct dense and loose areas. The addition of $Mo_{72}V_{30}$ increased the fracture energy of the hydrogel from 133 kJ·m^{-3} (QP) to 338 kJ·m^{-3} (QPP_{100}) (Fig. 2b), whereas the Young's modulus remained below 60 kPa because of the relatively low dosage, with the Young's modulus predominantly governed by chemical cross-linking and chain entanglement.[28] The modulus that matches that of biological soft tissue makes it more suitable for biomedical applications. The stress-strain curve of QP during the loading-unloading cycle (Fig. S3 in ESI) shows a relatively small hysteresis loop even at high strains because tension transmits along the chain and to many other chains through entanglement before the chain breaks.[31] After doping with $Mo_{72}V_{30}$, even smaller hysteresis loops can be observed (Fig. 2c), indicating that the energy dissipated as heat was negligible. These results also imply that QPP_{100} possesses superior resilience. Furthermore, the high swelling ratio eliminated temporary entanglements, which should also contribute to the extremely low hysteresis of the hydrogel.[36] Continuous loading-unloading cycle tests were conducted to evaluate the fatigue resistance of the hydrogels. As shown in Fig. 2(d) and Fig. S4(a) (in ESI), during the stretching cycles, the maximum stress of QPP_{100} remained almost the same and the residual strain was very low. The dissipated energy remained almost stable after the first decrease (Fig. S4b in ESI), indicating that the unstable sacrificial bonds or network structures within the material were rapidly reorganized and stabilized in the early stage and then entered a stable state with an efficient and reversible energy dissipation mechanism, which can effectively delay the accumulation of fatigue damage. These results show that the hydrogel has good fatigue resistance and stability. In addition, compared with QPP_{100}, the stress of QP decreased slightly at the 10th cycle (Fig. S5 in ESI), indicating enhanced elastic stability upon $Mo_{72}V_{30}$ incorporation. In addition to the tensile properties, the compressive behavior of the fully swollen hydrogels was examined. The QPP_{100} hydrogel exhibits a compressive stress of 2.63±0.08 MPa at a strain of 88% (Fig. 2e), demonstrating its ability to withstand large compressive deformation. A comparison of the fracture energy values for hydrogels with low Young's modulus reported in the literature is presented in Fig. 2(f), where many systems achieve high fracture energy at the expense of reduced water content.[37–45] In contrast, the present hydrogel system simultaneously maintained a high water content (>90%), high fracture energy, and low hysteresis. These properties can be primarily attributed to the synergistic effects of chain entanglement and appropriate introduction of POM-based physical crosslinking within the polymer network. Fig. 2(g) shows the images of QPP100 under different external forces. The material can be twisted, knotted, stretched, or compressed, and it can recover immediately after release.

Swelling Behavior and pH-/Ion-response

The swelling behavior of hydrogels provides a dynamic and tuneable interface that links their microscopic network structure with their macroscopic properties. By precisely regulating parameters such as the swelling ratio, swelling kinetics, and environmental responsiveness, hydrogels can be designed to exhibit tailored performance under different conditions. When the dried hydrogels were immersed in deionized water (Fig. 3a), all the samples reached swelling equilibrium within 5 h. Notably, the incorporation of $Mo_{72}V_{30}$ led to an increased swelling rate, which can be attributed to the enhanced hydrophilicity and water adsorption capability introduced by the POM clusters. In addition, under high-humidity atmosphere (85% relative humidity), the dried hydrogel exhibited measurable moisture uptake, with $Mo_{72}V_{30}$-doped samples showing a higher moisture absorption capacity (Fig. S6 in ESI).

The swelling behavior of hydrogels serves as a macroscopic and direct manifestation of the interaction between their internal microscopic network structure and external environment. Therefore, changes in SR are often employed to demonstrate the stimuli-responsive properties of hydrogels.[46] Based on its mechanical performance, QPP_{100} was chosen as the target hydrogel owing to its optimal mechanical properties. The pH sensitivity of hydrogels originates from the fact that the system contains groups that are easily hydrolyzed and protonated. The swelling behavior was observed by immersing the dried QPP_{100} hydrogel in solutions of different pH, and the results were recorded. As shown in Fig. S7 (in ESI), in acidic solutions, the charges of the cations $-N^+(CH_3)_3$ were shielded by the counter ions (Cl^-) through the screening effect, and their efficient repulsion was simultaneously prevented at the same time, thus lowering the SR. Under neutral conditions (pH=7), the internal environment of the hydrogel was almost unaffected by the absence of effects such as group protonation and deprotonation, thereby allowing rapid swelling of the hydrogel. In extremely basic solutions, the sharp increase in SR was caused by PAM hydrolysis. Fig. 3(b) shows the stable pH-responsive swelling behavior between 7 and 8 of the QPP_{100} hydrogel. The well-defined pH sensitivity reflects the balanced interplay between electrostatic interactions and network elasticity in the hydrogel system and highlights its potential for applications that require controllable swelling behavior.

We selected 6 commonly used salts to monitor the re-

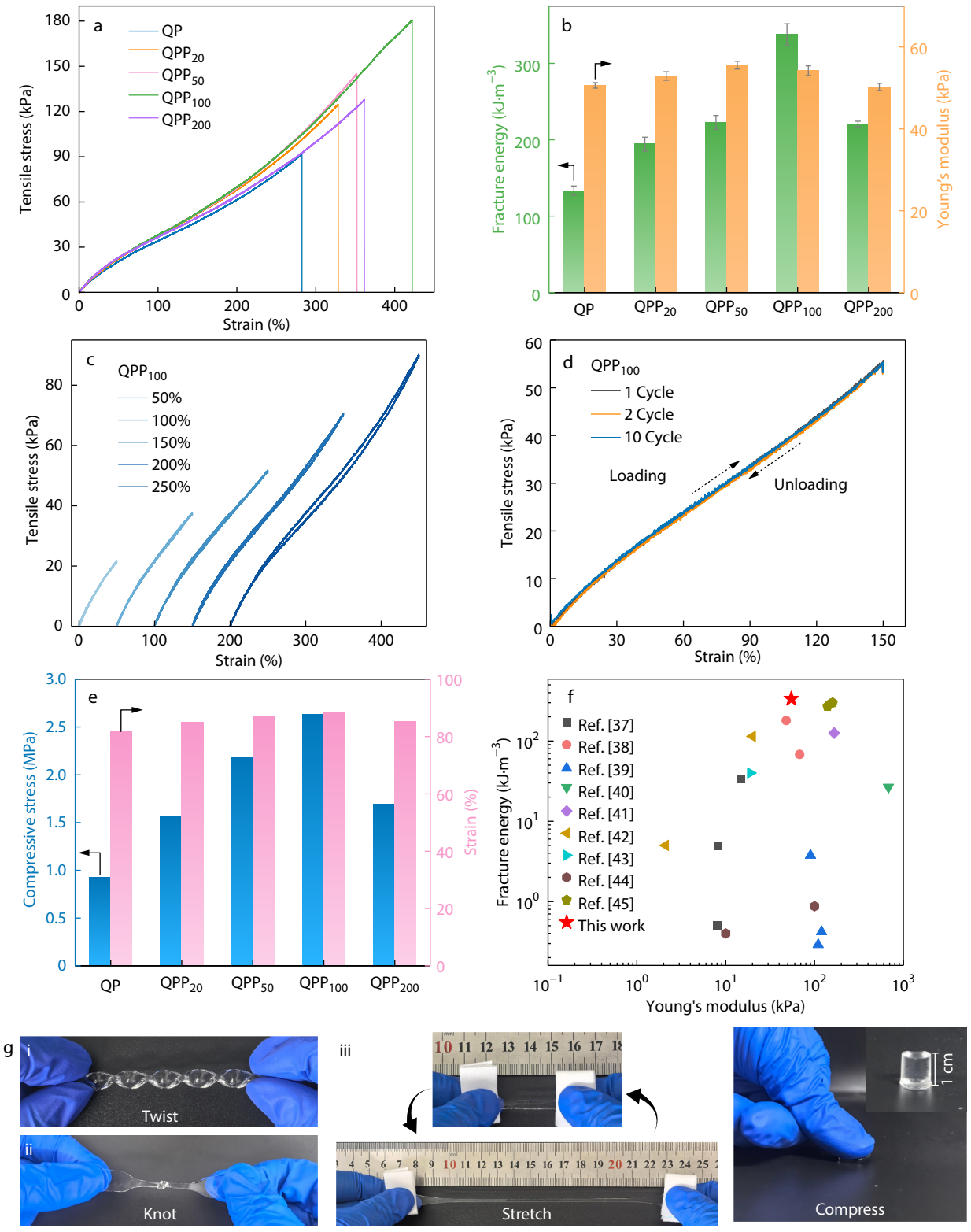

Fig. 2 (a) Tensile stress-strain curves of QP and QPP hydrogels; (b) Fracture energy and Young's modulus of QP and QPP hydrogels; (c) Loading-unloading tensile curves of QPP_{100} under different strains; (d) Fatigue resistance performance of QPP_{100}; (e) Compressive strength and ultimate strain of QP and QPP hydrogels; (f) Fracture energy chart compared with reported hydrogels; (g) The twisted (i), knoted (ii), stretched (iii) and compressed (iv) images of water equilibrium QPP_{100}.

https://doi.org/10.1007/s10118-026-3611-z

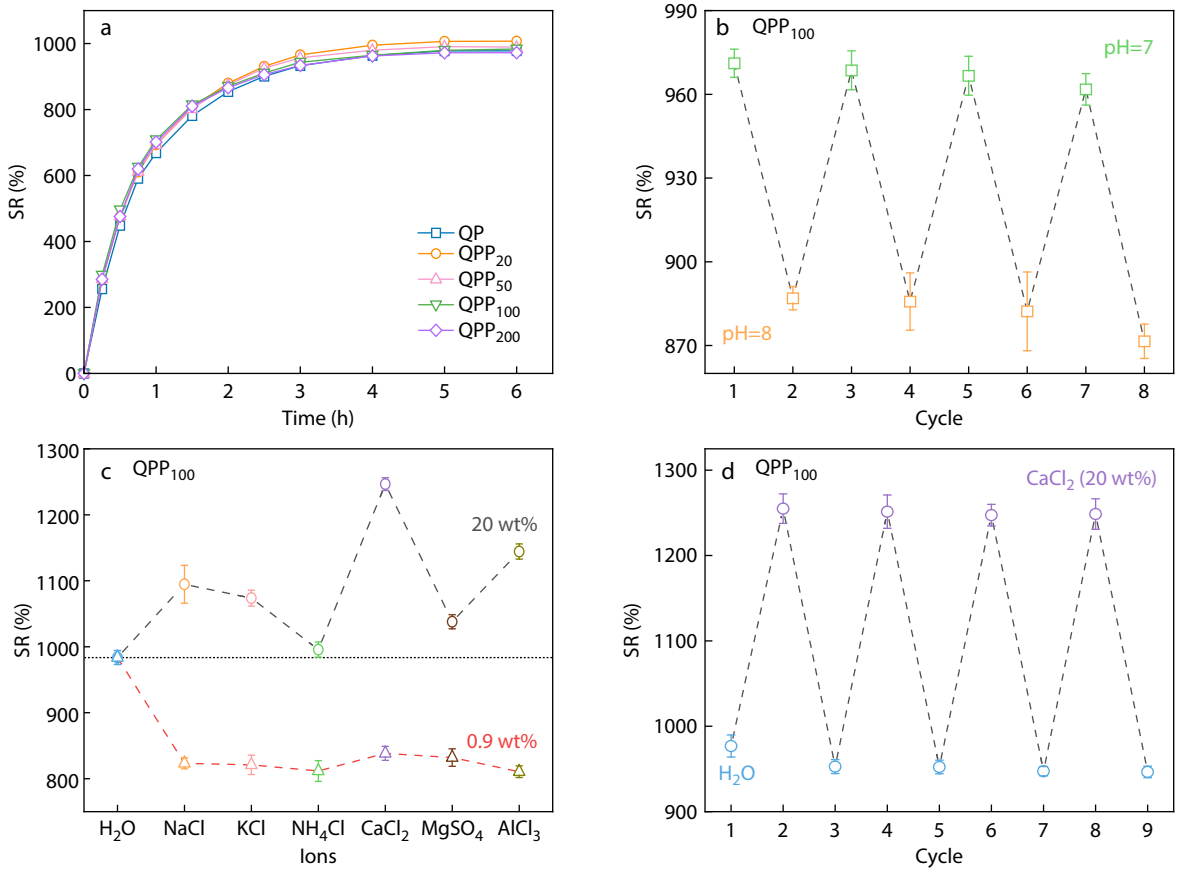

Fig. 3 (a) Swelling kinetic curves of QP and QPP hydrogels in deionized water; (b) Stability of QPP_{100} response to pH; (c) The SR of QPP_{100} in different salt solutions (concentration: 0.9 wt% and 20 wt%); (d) Stability of QPP_{100} response to $CaCl_2$.

sponse of hydrogels to ions. When immersed in six 0.9 wt% salt solutions, the SR of QPP_{100} decreased by approximately 14.7%–17.5% compared to that in deionized water (Fig. 3c). This is because, in low-concentration salt solutions, the cations dissociated from the salt form ion-dipole interactions with the amide carbonyl oxygens (negative charge), while the anions may form hydrogen bonds with the amide hydrogen atoms (positive charge).[47–49] Additionally, the electrostatic repulsion between the positively charged quaternary ammonium groups is shielded, and the external osmotic pressure increases. Therefore, the polymer network shrinks and the water molecules migrate outward. However, as shown in Fig. 3(c), after soaking the QPP_{100} hydrogel in several 20 wt% high-concentration salt solutions, the SR changed significantly, demonstrating its sensitivity to different ions. Furthermore, compared to immersion in deionized water, the hydrogel exhibited an increase in swelling ratio in all high-concentration salt solutions, reaching up to 26.9% in $CaCl_2$ solution. This phenomenon typically occurs in polyzwitterionic hydrogels owing to the antipolyelectrolyte effect.[50,51] The difference is that the QPP_{100} hydrogel can only occur at a higher concentration (15 wt%–20 wt%) (Fig. S8 in ESI), whereas typical polyzwitterionic hydrogels can significantly increase at a lower concentration of 5 wt%. In the QPP hydrogel system, a high concentration of external ions in the salt solution flows into the network to balance the concentration gradient. Some functional groups within the network interact with these ions, restricting their outward diffusion and thereby creating osmotic pressure from the inside to the outside. In addition, a high ion concentration weakens the interactions between the polymer chains. As a result, the hydrogel exhibited an increased swelling degree in highly concentrated salt solutions. Fig. 3(d) shows the cyclic swelling behavior of QPP_{100} in deionized water and $CaCl_2$ solution (20 wt%), which has the highest SR, indicating that the hydrogel possesses favorable stability in its stimulus-responsive performance. This unique salt-responsive behavior holds promise for applications in smart drug delivery systems and salinity sensors, especially for seawater desalination systems.

Tribological Performance

The lubricating properties of hydrogels, a key core characteristic, serve as a vital bridge connecting materials science with life sciences and flexible electronics. Researchers typically employ strategies, such as network structure modulation, interface engineering, and fabrication process optimization, to enhance the lubricating performance of hydrogels. As shown in Fig. 4(a) and Fig. S9 (in ESI), with the increase in $Mo_{72}V_{30}$ addition, the coefficient of friction first decreased and then increased, reaching a minimum of 0.09 at an addition level of 100 ppm. This was attributed to $Mo_{72}V_{30}$ acting as a physical cross-linking point, which densifies and homogenizes the hydrogel network. Furthermore, the metal centers of POMs possess strong electron-accepting capabilities, enabling coordination interactions with oxygen atoms in water molecules. The abundant bridging and

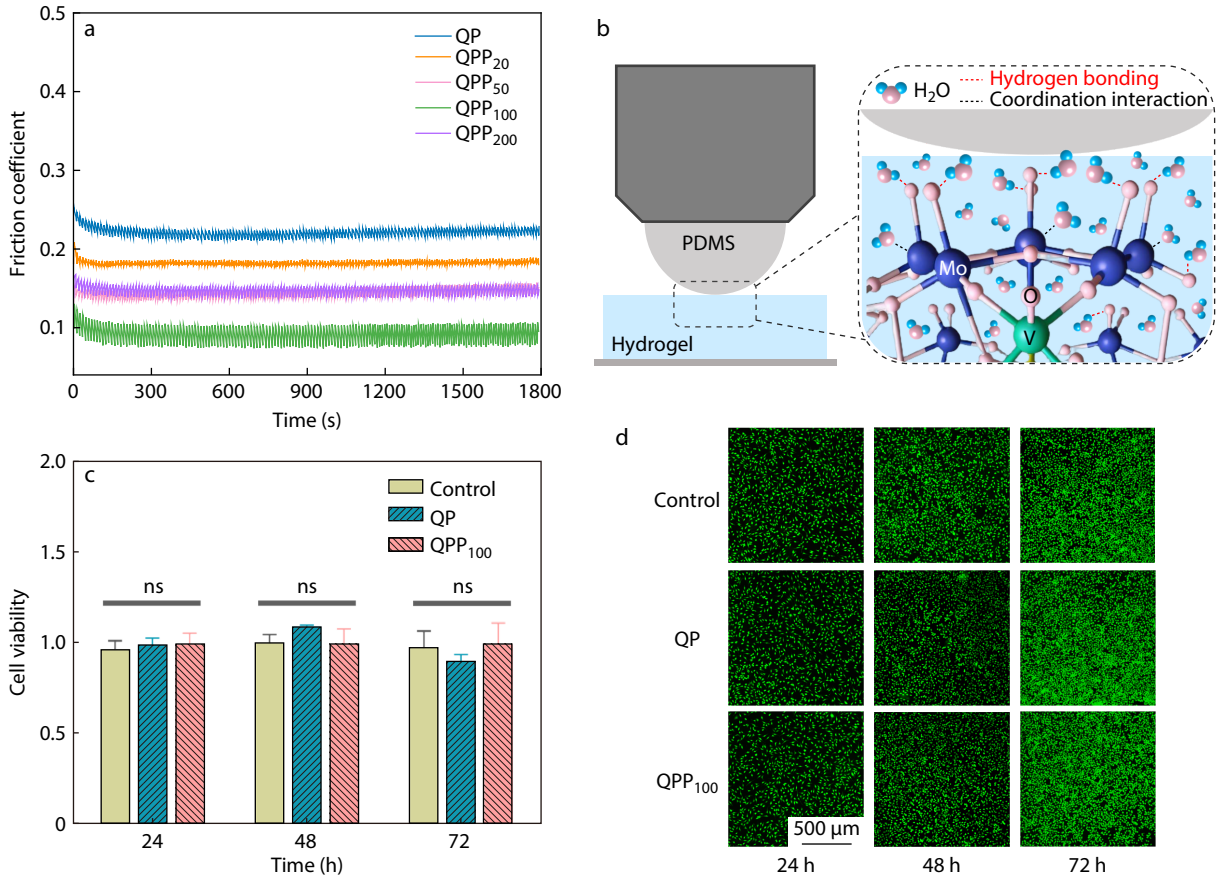

Fig. 4 (a) Effect of $Mo_{72}V_{30}$ doping on friction properties of hydrogels (frequency: 1 Hz; load: 0.5 N; friction pair: PDMS); (b) Multiple interactions between water molecules and $Mo_{72}V_{30}$ in hydrogels; (c) Relatively cell viability of L929 cells after incubation with hydrogel extract (0.1 g·mL^{-1}) for 24, 48, and 72 h (ns stands for no significant difference); (d) Live/Dead fluorescence images of L929 cells after incubation with hydrogel extracts for 24, 48 and 72 h (0.1 g·mL^{-1}).

terminal oxygen atoms in the POMs structure can form strong hydrogen bonds with water molecules, thereby "blocking" the water molecules within the structure and forming a hydrated layer (Fig. 4b).[52,53] This layer reduced the interfacial shear resistance during friction. In addition, in the low-speed region, the friction coefficient of QPP_{100} remained almost unchanged with the frequency (Fig. S10 in ESI). After turning the lubricant into a high-concentration urea solution (8 mol·L^{-1}), the friction coefficient rapidly increased within a few minutes and then gradually stabilized, which was attributed to the disruption of the hydration layer and hydrogen-bonding network by urea. These results collectively indicate that the friction behavior is dominated by boundary lubrication *via* the hydrated layer. Although excessive $Mo_{72}V_{30}$ incorporation is not conducive to the uniformity of the hydrogel network, which leads to a slight increase in the friction coefficient as a secondary factor, it is still better than that of the QP hydrogel. These results indicate that POMs may serve as an ideal class of dopants to enhance the lubrication performance of hydrogel materials.

Biocompatibility

Considering the potential applications of hydrogels in biological environments, their biocompatibility was evaluated, with a particular focus on $Mo_{72}V_{30}$. The cytocompatibility of the QP and QPP hydrogels was assessed by CCK-8 assay using L929 fibroblast cells. As illustrated in Figs. 4(c) and 4(d), both the QP and QPP_{100} hydrogels exhibit high cell viability after co-culture with L929 cells, with values consistently exceeding 90%. These results indicated that the introduction of $Mo_{72}V_{30}$ at the investigated concentration did not induce detectable cytotoxicity and did not adversely affect the intrinsic biocompatibility of the hydrogel system. The favorable cell viability further suggests that $Mo_{72}V_{30}$ can be incorporated into the hydrogel network without compromising cytocompatibility.

CONCLUSIONS

In summary, $Mo_{72}V_{30}$ was incorporated into chitosan quaternary ammonium/polyacrylamide (QP) hydrogels as an additional physical crosslinking component to construct an interpenetrating and entangled network structure. The resulting QPP_{100} hydrogel exhibited excellent tensile properties (422%), high fracture energy (338 kJ·m^{-3}), negligible hysteresis accompanied by rapid elastic recovery, while maintaining a high water content exceeding 90%. Simultaneously, the incorporation of $Mo_{72}V_{30}$ effectively reduced the friction coefficient of the hydrogel owing to its strong water-adsorption capacity and the formation of a dense and homogeneous hydrogel network. Furthermore, the QPP hydrogels demonstrated pH- and ion-responsive swelling behaviors with stable cyclic performance

under varying external stimuli. These results demonstrate that polyoxometalates can function as effective physical crosslinking agents in hydrogel systems, providing a viable strategy for simultaneously achieving a high water content, mechanical robustness, and tunable interfacial properties.

Conflict of Interests

The authors declare no interest conflict.

Electronic Supplementary Information

Electronic supplementary information (ESI) is available free of charge in the online version of this article at http://doi.org/10.1007/s10118-026-3611-z.

Data Availability Statement

Data supporting the findings of this study are available from the corresponding author upon reasonable request. Author's contact information: shengwb@licp.cas.cn and zhm@licp.cas.cn.

ACKNOWLEDGMENTS

This work was financially supported by Gansu Province Postdoctoral Research Funding 24-25.

REFERENCES

1 Wichterle, O.; Lím, D. Hydrophilic gels for biological use. *Nature* **1960**, *185*, 117–118.
2 Zhao, X., Chen, X.; Yuk, H.; Lin, S.; Liu, X.; Parada, G. Soft materials by design: Unconventional polymer networks give extreme

Graphical Abstract

Polyoxometalate-doped Chitosan Quaternary Ammonium/Polyacrylamide Interpenetrating Hydrogels with Enhanced Mechanical and Tribological Properties

Fang Xu, Xin-Bao Han, Hao-Hao Ren, Wei-Tao Gong, Rong-Sheng Cai, Yu Li, Ming Zhang, and Wen-Bo Sheng

Lanzhou Institute of Chemical Physics, Chinese Academy of Sciences; Lanzhou University; Shandong Laboratory of Advanced Materials and Green Manufacturing at Yantai

Polyoxometalate (POM) doped chitosan quaternary ammonium/polyacrylamide hydrogel with chain entanglement has enhanced mechanical properties (low hysteresis and excellent resilience), improved lubrication performance, and multiple responsiveness to pH and salt ions.

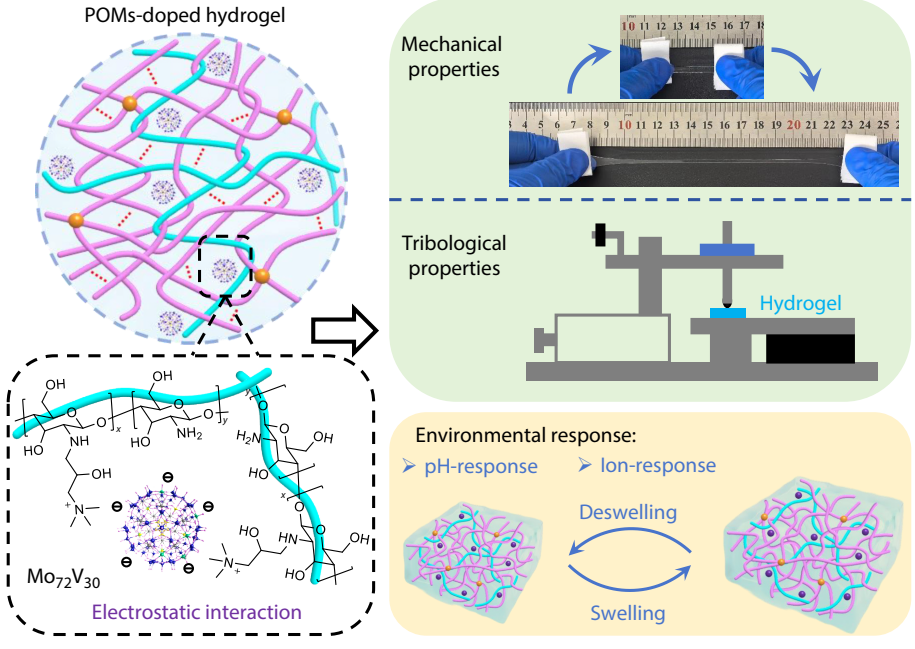

Chinese J. Polym. Sci., 2026 *https://doi.org/10.1007/s10118-026-3611-z*

properties. *Chem. Rev.* **2021**, *121*, 4309–4372.
3 Chen, W.; Ming, Y.; Wang, M.; Huang, M.; Liu, H.; Huang, Y.; Huang, Z.; Qing, L.; Wang, Q.; Jia, B. Nanocomposite hydrogels in regenerative medicine: applications and challenges. *Macromol. Rapid Commun.* **2023**, *44*, 2300128.
4 Wang, Q.; Kang, M.; Wang, D.; Tang, B. Z. Synergizing AIE luminogens and hydrogel matrices: advancing precision medicine through smart material design. *Coord. Chem. Rev.* **2026**, *548*, 217227.
5 Imani, K. B. C.; Dodda, J. M.; Yoon, J.; Torres, F. G.; Imran, A. B.; Deen, G. R.; Al-Ansari, R. Seamless integration of conducting hydrogels in daily life: from preparation to wearable application. *Adv. Sci.* **2024**, *11*, 2306784.
6 Yang, S.; Yang, Y.; Xia, X.; Zou, B.; Wang, B.; Zhang, Y. Biomimetic stimulus responsiveness: from materials design to device integration. *Adv. Funct. Mater.* **2024**, *34*, 2400500.
7 Verma, A.; Lal, B.; Ravi, K.; Suman; Ramya, M.; Singh, S.; Jasrotia, R. Clean water future: the role of chitosan hydrogel nanocomposites in wastewater management. *Int. J. Biol. Macromol.* **2025**, *330*, 148213.
8 Zhang, Z.; Fu, H.; Li, Z.; Huang, J.; Xu, Z.; Lai, Y.; Qian, X.; Zhang, S. Hydrogel materials for sustainable water resources harvesting & treatment: synthesis, mechanism and applications. *Chem. Eng. J.* **2022**, *439*, 135756.
9 Zou, L.; Li, Y.; Feng, S.; Wang, Z.; Xiao, H.; Chen, S.; Wang, Y.; He, L.; Mao, X. Innovations and applications of composite hydrogels: from polymer-based systems to metal-ion-doped and functional nanomaterial-enhanced architectures. *Small* **2025**, *21*, 2503147.
10 Zuo, F.; Hu, J.; Zhang, S. X.; Guo, J. X.; Li, R. G.; Xin, Y. M.; Li, C. J.; Yan, J. Q. Facile preparation of super-strong and tough poly(vinyl alcohol)/carbon nanotube hydrogel enabled by triple crosslinking networks. *Chinese J. Polym. Sci*. **2025**, DOI: 10.1007/s10118-025-3438-z.
11 Wei, K.; Yu, X.; Zhang, X.; Cao, J.; Bai, L.; Wang, W.; Chen, H.; Yang, L. Self-healing, tough hydrogels with long-lasting moisture and extreme temperature tolerance and application for flexible sensors. *Chem. Eng. Sci.* **2026**, *319*, 122312.
12 Wang, Y.; Li, Y.; Zhang, Y.; You, L.; Song, Y.; Li, T.; Fang, Z.; Gui, A.; Li, Y.; Liao, L.; Yang, R. Graphene-doped hydrogels with enhanced conductivity and stretchability for all-weather wearable devices. *Adv. Funct. Mater.* **2025**, *35*, 2425014.
13 Tang, Y.; Wu, B.; Li, J.; Lu, C.; Wu, J.; Xiong, R. Biomimetic structural hydrogels reinforced by gradient twisted plywood architectures. *Adv. Mater.* **2024**, *37*, 2411372.
14 Zeng, X.; Teng, L.; Wang, X.; Lu, T.; Leng, W.; Wu, X.; Li, D.; Zhong, Y.; Sun, X.; Zhu, S.; Dong, Y.; Tan, P.; Zeng, Z.; Hu, Z.; Li, Z.; Zheng, Q. Efficient multi-physical crosslinked nanocomposite hydrogel for a conformal strain and self-powered tactile sensor. *Nano Energy* **2025**, *135*, 110669.
15 Guo, J.; Zhang, T.; Hao, X.; Liu, S.; Zou, Y.; Li, J.; Wu, W.; Chen, L.; Liu, X. Aramid nanofiber/MXene-reinforced polyelectrolyte hydrogels for absorption-dominated electromagnetic interference shielding and wearable sensing. *Nano-Micro Lett.* **2025**, *17*, 271.
16 Pardo, A.; Gómez-Florit, M.; Barbosa, S.; Taboada, P.; Domingues, R. M. A.; Gomes, M. E. Magnetic nanocomposite hydrogels for tissue engineering: design concepts and remote actuation strategies to control cell fate. *ACS Nano* **2021**, *15*, 175–209.
17 Wang, M.; Ouyang, R.; Jiang, Y.; Liu, Z.; Zhou, X.; Shi, Y.; He, C.; Zhu, L.; Yue, B. Conductive hydrogels with photothermal effects: material design, mechanisms, and multifunctional applications. *Sci. China Chem.* **2025**, *68*, 4693–4711.
18 Fang, Y.; Xing, C.; Liu, J.; Zhang, Y.; Li, M.; Han, Q. Supermolecular film crosslinked by polyoxometalate and chitosan with superior antimicrobial effect. *Int. J. Biol. Macromol.* **2020**, *154*, 732–738.
19 Ma, M.; Li, C.; Fan, W.; Su, Y.; Guo, D.; Li, M.; Zhou, Y. Constructing high-efficiency polyoxometalate-based antibacterial hydrogels for wearable sensors. *Langmuir* **2025**, *41*, 26261–26275.
20 Yang, D.; Wang, M.; Sun, L.; Ma, P. A tetrameric double peroxyl bonds-bridged Zr-substituted phosphotungstate with good catalytic oxidation activity for sulfides. *Mol. Catal.* **2025**, *572*, 114786.
21 Mu, C.; Fang, J.; Nie, J.; Fu, L.; Li, W. Embedding hydrogel electrodes into hydrogel electrolyte: an 3D protecting strategy for stretchable high-performance supercapacitor. *Chem. Eng. J.* **2024**, *484*, 149505.
22 Geng, J.; Lu, Y.; Yang, J.; Xue, S.; Meng, Y.; Liu, S. A polyoxometalate-based multifunctional hydrogel for integrated electrochromic and sensing devices. *Chem. Eng. J.* **2025**, *511*, 161798.
23 Guedes, G.; Wang, S.; Fontana, F.; Figueiredo, P.; Lindén, J.; Correia, A.; Pinto, R. J. B.; Hietala, S.; Sousa, F. L.; Santos, H. A. Dual-crosslinked dynamic hydrogel incorporating $\{Mo_{154}\}$ with pH and NIR responsiveness for chemo-photothermal therapy. *Adv. Mater.* **2021**, *33*, 2007761.
24 Dutta, S.; Misra, A.; Bose, S. Polyoxometalate nanocluster-infused triple IPN hydrogels for excellent microplastic removal from contaminated water: detection, photodegradation, and upcycling. *Nanoscale* **2024**, *16*, 5188–5205.
25 Zhao, B.; Ren, Y.; Zhang, K.; Dong, Y.; Wang, K.; Zhang, N.; Li, J.; Yuan, M.; Wang, J.; Tu, Q. Hydroxypropyl methylcellulose reinforced bilayer hydrogel dressings containing L-arginine-modified polyoxometalate nanoclusters to promote healing of chronic diabetic wounds. *Carbohyd. Polym.* **2024**, *342*, 122396.
26 Liu, C.; Lv, M.; Xu, Q.; Xie, J.; You, Y.; Guo, K.; Jiang, G.; Hou, L.; Yang, H.; Yong, Y. Chronological adaptive polyoxometalate-based hydrogel for diabetic chronic wounds through synchronous bacterial ferroptosis death and immuno-modulation. *Nano Today* **2024**, *58*, 102415.
27 Huang, H.; Su, Y.; Wang, C.; Lei, B.; Song, X.; Wang, W.; Wu, P.; Liu, X.; Dong, X.; Zhong, L. Injectable tissue-adhesive hydrogel for photothermal/chemodynamic synergistic antibacterial and wound healing promotion. *ACS Appl. Mater. Interfaces* **2023**, *15*, 2714–2724.
28 Xu, F.; Han, X.; Xu, R.; Ren, H.; Ma, S.; Li, B.; Wu, Y.; Zhou, F.; Sheng, W. Hydrogels with negligible hysteresis, enhanced conductivity, and good absorbability enabled by synergistic chain entanglement and polyoxometalates. *ACS Appl. Mater. Interfaces* **2025**, DOI: 10.1021/acsami.5c18803.
29 Müller, A.; Todea, A. M.; van Slageren, J.; Dressel, M.; Bögge, H.; Schmidtmann, M.; Luban, M.; Engelhardt, L.; Rusu, M. Triangular geometrical and magnetic motifs uniquely linked on a spherical capsule surface. *Angew. Chem. Int. Ed.* **2005**, *44*, 3857–3861.
30 Botar, B.; Kögerler, P.; Hill, C. L. $[\{(Mo)Mo_5O_{21}(H_2O)_3(SO_4)\}_{12}(VO)_{30}(H_2O)_{20}]^{36-}$: a molecular quantum spin icosidodecahedron. *Chem. Commun*. **2005**, *25*, 3138–3140.
31 Kim, J.; Zhang, G.; Shi, M.; Suo, Z. Fracture, fatigue, and friction of polymers in which entanglements greatly outnumber cross-links. *Science* **2021**, *374*, 212–216.
32 Zhao, J.; Chen, R.; Cheng, D.; Yang, X.; Zhang, H.; Zheng, J.; Hu, R. Extremely ultrahigh stretchable starch-based hydrogels with continuous hydrogen bonding. *Adv. Funct. Mater.* **2025**, *35*, 2415530.
33 Wang, H.; Fang, L.; Yang, Y.; Zhang, L.; Wang, Y. $H_5PMo_{10}V_2O_{40}$ immobilized on functionalized chloromethylated polystyrene by electrostatic interactions: a highly efficient and recyclable heterogeneous catalyst for hydroxylation of benzene. *Catal. Sci. Technol.* **2016**, *6*, 8005–8015.
34 Xiao, W.; Zhao, P.; Deng, S.; Zhang, N. Anchoring $H_3PW_{12}O_{40}$ on 3-

aminopropyltriethoxysilane modified graphene oxide: enhanced adsorption capacity and photocatalytic activity toward methyl orange. *New J. Chem.* **2015**, *39*, 3719–3727.
35 Petchsangsai, M.; Sajomsang, W.; Gonil, P.; Nuchuchua, O.; Sutapun, B.; Puttipipatkhachorn, S.; Ruktanonchai, U. R. A water-soluble methylated *N*-(4-*N*,*N*-dimethylaminocinnamyl) chitosan chloride as novel mucoadhesive polymeric nanocomplex platform for sustained-release drug delivery. *Carbohyd. Polym.* **2011**, *83*, 1263–1273.
36 Meng, X.; Qiao, Y.; Do, C.; Bras, W.; He, C.; Ke, Y.; Russell, T. P.; Qiu, D. Hysteresis-free nanoparticle-reinforced hydrogels. *Adv. Mater.* **2022**, *34*, 2108243.
37 Lan, G.; Zhu, S.; Chen, D.; Zhang, H.; Zou, L.; Zeng, Y. Highly adhesive antibacterial bioactive composite hydrogels with controllable flexibility and swelling as wound dressing for full-thickness skin healing. *Front. Bioeng. Biotech.* **2021**, *9*, 785302.
38 Xia, S.; Fu, W.; Liu, J.; Gao, G. Recyclable hydrogel for human-machine interface of multi-mode human vital signal acquisition. *Sci. China Mater.* **2023**, *66*, 2843–2851.
39 Huang, S. C.; Xia, X. X.; Fan, R. X.; Qian, Z. G. Programmable electrostatic interactions expand the landscape of dynamic functional hydrogels. *Chem. Mater.* **2020**, *32*, 1937–1945.
40 Viboonratanasri, D.; King, D. R.; Okumura, T.; Terkawi, M. A.; Katsuyama, Y.; Lama, M.; Yasui, T.; Kurokawa, T. Porous and tough polyacrylamide/carboxymethyl cellulose gels chemically crosslinked *via* Cryo-UV polymerization for sustained drug release. *Gels* **2025**, *11*, 453.
41 Wang, F.; Song, X.; Chen, J.; Chu, J.; Wang, Y.; Chen, Y. Mechanically robust, high water-content hydrogels with microphase separated membrane for wastewater regeneration. *Colloids Surf. A: Physicochem. Eng. Asp.* **2026**, *730*, 138953.
42 Feng, Y.; Wang, S.; Li, Y.; Ma, W.; Zhang, G.; Yang, M.; Li, H.; Yang, Y.; Long, Y. Entanglement in smart hydrogels: fast response time, anti-freezing and anti-drying. *Adv. Funct. Mater.* **2023**, *33*, 2211027.
43 Zhang, M.; Yang, Y.; Li, M.; Shang, Q.; Xie, R.; Yu, J.; Shen, K.; Zhang, Y.; Cheng, Y. Toughening double-network hydrogels by polyelectrolytes. *Adv. Mater.* **2023**, *35*, 2301551.
44 Park, J.; Kim, J. Y.; Heo, J. H.; Kim, Y.; Kim, S. A.; Park, K.; Lee, Y.; Jin, Y.; Shin, S. R.; Kim, D. W.; Seo, J. Intrinsically nonswellable multifunctional hydrogel with dynamic nanoconfinement networks for robust tissue-adaptable bioelectronics. *Adv. Sci.* **2023**, *10*, 2207237.
45 Lin, X.; Zhang, L.; Duan, B. Polyphenol-mediated chitin self-assembly for constructing a fully naturally resourced hydrogel with high strength and toughness. *Mater. Horiz.* **2021**, *8*, 2503–2512.
46 Zhang, Y.; Wei, H.; Hua, B.; Hu, C.; Zhang, W. Preparation and application of the thermo-/pH-/ion-sensitive semi-IPN hydrogel based on chitosan. *Int. J. Biol. Macromol.* **2024**, *258*, 128968.
47 Qiu, W.; Chen, G.; Zhu, H.; Zhang, Q.; Zhu, S. Enhanced stretchability and robustness towards flexible ionotronics *via* double-network structure and ion-dipole interactions. *Chem. Eng. J.* **2022**, *434*, 134752.
48 Huang, X. Y.; Zhu, H. Q.; Li, L. F.; Lv, T. C.; Li, H. Y.; Gu, J. J.; Wang, W.; Xue, B.; Lei, H.; Cao, Y. Tough, transparent, self-healing ionogel with exceptional moisture and impact resistance. *Chinese J. Polym. Sci.* **2025**, *43*, 1483–1495.
49 Yao, P.; Bao, Q.; Yao, Y.; Xiao, M.; Xu, Z.; Yang, J.; Liu, W. Environmentally stable, robust, adhesive, and conductive supramolecular deep eutectic gels as ultrasensitive flexible temperature sensor. *Adv. Mater.* **2023**, *35*, 2300114.
50 Zheng, S. Y.; Zhou, J.; Si, M.; Wang, S.; Zhu, F.; Lin, J.; Fu, J.; Zhang, D.; Yang, J. A molecularly engineered zwitterionic hydrogel with strengthened anti-polyelectrolyte effect: from high-rate solar desalination to efficient electricity generation. *Adv. Funct. Mater.* **2023**, *33*, 2303272.
51 Zeng, J.; Chen, H.; Dong, L.; Guo, X. Anti-polyelectrolyte effect of zwitterionic hydrogel electrolytes enabling high-voltage zinc-ion hybrid capacitors. *Adv. Funct. Mater.* **2024**, *34*, 2314651.
52 Zhang, H.; Wang, Y.; Shi, Y.; Zhang, Y.; Yang, Y.; Wang, Y.; Cui, Y.; Guo, J.; Zhang, P.; Sun, L.; Zhang, J. Recent advances in polyoxometalate-based proton conducting materials: design strategies, conduction mechanisms, structure-function relationships and future perspectives. *Nano Res.* **2025**, *18*, 94907743.
53 Jin, D.; Qiao, F.; Zhou, Y.; Wang, J.; Cao, K.; Yang, J.; Zhao, J.; Zhou, L.; Li, H. Cu/Mo_2C synthesized through Anderson-type polyoxometalates modulate interfacial water structure to achieve hydrogen evolution at high current density. *Nano Res.* **2023**, *17*, 2546–2554.

https://doi.org/10.1007/s10118-026-3611-z